MOLECULAR IMAGING AND BIOLOGY

Mol Imaging Biol (2019) 21:965–972
DOI: 10.1007/s11307-018-1299-3

Published Online: 26 November 2018

RESEARCH ARTICLE

Prognostic Impact of Intratumoral Heterogeneity Based on Fractal Geometry Analysis in Operated NSCLC Patients

Angelo Castello,[1] Carlo Russo,[2] Fabio Grizzi,[3] Dorina Qehajaj,[3] Egesta Lopci[1]

[1]*Department of Nuclear Medicine, Humanitas Clinical and Research Hospital, Via Manzoni 56, 20089, Rozzano, MI, Italy*
[2]*Michele Rodriguez Foundation, Milan, Italy*
[3]*Department of Immunology and Inflammation, Humanitas Clinical and Research Hospital, Rozzano, MI, Italy*

Abstract

Purpose: To determine the heterogeneity of glucose uptake applying fractal analysis on positron emission tomography/computed tomography (PET/CT) with 2-deoxy-2-[^{18}F]fluoro-D-glucose ([^{18}F]FDG) images in patients with non-small cell lung carcinoma (NSCLC) before surgery, and to assess whether this heterogeneity was associated with disease-free survival (DFS).

Procedures: [^{18}F]FDG PET/CT scans of 113 patients' prior surgery were retrospectively revised. PET DICOM images were analyzed for fractal geometry using a *ad hoc* software to automatically determine the following indexes: (a) mean intensity value (MIV), (b) standard deviation (SD), (c) relative dispersion (RD), (d) three-dimensional (3D) histogram of the fractal dimension (3D HIST FR DIM), and (e) fractal dimension in 3D (3D-FD). All the fractal indexes were subsequently compared with metabolic parameters and disease-free survival (DFS).

Results: We found a significant correlation between 3D-FD and SUVmax, SUVmean, MTV, and TLG. Additionally, positive correlations between MIV, SD, and all metabolic parameters were also detected. Patients with high 3D-FD tumor (≥ 1.62) showed significantly higher values of SUVmax, SUVmean, MTV, and TLG than those with lower 3D-FD. In univariate analysis, median 3D-FD and median TLG were significantly associated with DFS ($p = 0.04$ and $p = 0.03$, respectively). These findings were confirmed on log-rank test. On multivariate analysis, among age, stage disease, histotype, 3D-FD, and metabolic parameters, only 3D-FD was identified as independent prognostic factor for DFS ($p = 0.032$; HR 0.418, 95 % CI 0.189–0.926). 3D-FD was different between adenocarcinoma and squamous cell carcinoma (1.60 *versus* 1.88, $p = 0.014$), and 3D-FD value was found higher in advanced stage disease.

Conclusions: Metabolic heterogeneity determined applying fractal principles on PET images can be considered as a novel imaging biomarker for survival in patients with NSCLC.

Key Words: NSCLC, Heterogeneity, Fractals, Geometry, [^{18}F]FDG PET/CT, Disease-free survival

Introduction

Lung cancer represents the first cause of cancer-related death, despite continuous progresses in diagnosis and therapy. Non-small cell lung carcinoma (NSCLC) accounts for 80–85 % of all cases of lung cancer [1]. One of the main issues with lung cancer is related to the absence of pain or symptoms complained by patients, so that early diagnosis appears tough. This explains why almost half of the patients present with locally advanced or metastatic disease at

Correspondence to: Egesta Lopci; *e-mail:* egesta.lopci@humanitas.it; *e-mail:* egesta.lopci@gmail.com

diagnosis, having an estimated overall 5-year survival rate of 18 % [1, 2]. Therefore, the development of more-effective diagnostic, therapeutic, and surveillance tools is needed and should represent the goal for the future lung cancer research.

In the last years, positron emission tomography/x-ray computed tomography (PET/CT) with 2-deoxy-2-[^{18}F]fluoro-D-glucose ([^{18}F]FDG) has gained a primary role in the lung cancer management. Combining anatomical localization and morphological information with metabolic data, [^{18}F]FDG PET/CT can detect pulmonary lesions with a high sensitivity (94 %) and specificity (83 %) [3–5]. Maximum standardized uptake value (SUVmax) is a metabolic parameter that reflects the highest degree of FDG uptake. However, its distribution within the tumor is not homogenous due to the presence of necrosis, angiogenesis, hypoxia, and proliferative phenomena [6]. Recent studies have demonstrated that heterogeneous glucose metabolism measured on [^{18}F]FDG PET/CT images is associated with the clinical outcome of various types of cancer. As a consequence, the assessment of tumor heterogeneity by imaging could help characterize structural heterogeneity and provide prognostic information [7–9].

In biology, as well as in oncology, we are often presented with the complexity of cellular systems, which classical Euclidean geometry cannot explain [10]. Fractal analysis is a non-compartment model that can be applied to digital images in order to estimate their heterogeneity and complexity, expressed by a non-integer number, named fractal dimension (FD) [11, 12]. In other papers, it has been demonstrated that mean FD varies according to differentiation grade (*i.e.*, G1-G3) of endometriod endometrial adenocarcinoma [13], whereas bone metastases from renal, breast and lung tumors had multifractal parameters significantly different for all three considered groups, providing an aid for clinicians in case of primitive occult tumors [14]. To date, few investigators have examined the association between FD applied on PET/CT images and lung tumors [15–17]. Therefore, it is reasonable to explore FD along with "traditional" [^{18}F]FDG PET/CT parameters in order to obtain additional information that might improve the clinical decision process.

In this study, we aimed to determine the heterogeneity of glucose uptake applying fractal analysis on [^{18}F]FDG PET/CT images in patients with non-small cell lung carcinoma (NSCLC) before surgery, and to assess whether this feature was associated with disease-free survival (DFS).

Materials and Methods

Patient Population

This retrospective study was conducted with the approval of the local Ethics Committee of our Institution and according to the Helsinki Declaration, and informed consent was obtained from all patients. We designed a retrospective analysis of all patients referred to our institution for surgical resection of NSCLC. From October 2010 to March 2017, 113 patients (77 male, 36 female; median age 70 years, range 44–90 years) were revised. Inclusion criteria comprised age older than 18 years, histopathological proven NSCLC, and staging [^{18}F]FDG PET/CT performed at our institution before surgery. The baseline epidemiologic and clinical characteristics of the study population are shown in Table 1.

[^{18}F]FDG PET/CT

PET/CT scans were performed according to standard procedures [18]. All patients fasted for at least 6 h before intravenous injection of [^{18}F]FDG (250–500 MBq), and scanning began 60 min later. [^{18}F]FDG PET/CT images were acquired with two hybrid scanners: Siemens Biograph LSO (Siemens Erlangen; Munich, Germany) and Discovery 690 (General Electric Healthcare; Waukesha, Wisconsin, USA). The scanners used in this study are accredited by the EANM Research Ltd. (EARL) program, and the image analysis was carried out using standardized acquisitions [18]. All PET images were attenuation corrected (CT 120 kV, 30 mA). Iterative image reconstruction was based on the ordered subsets expectation maximization (OSEM) algorithm with 6 iterations and 12 subsets. Reconstructed images were then displayed on a GE ADW4.6 workstation (GE Healthcare, Waukesha, Wisconsin, USA) and interpreted by experienced nuclear medicine physicians.

Table 1. Main patients' characteristics

	No (%)
Age median [range]	70 [44–90]
Gender	
Male	77 (68.1)
Female	36 (31.9)
Smoking history	
Yes	46 (40.7)
No	21 (18.6)
Former	46 (40.7)
TNM (8th edition)	
pT stage	
1	31 (27.4)
2	49 (43.4)
3	27 (23.9)
4	6 (5.3)
pN negative	71 (62.8)
pN positive	42 (37.2)
Cancer stage	
IA-IB	47 (41.6)
IIA-IIB	38 (33.6)
IIIA-IIIB	28 (24.8)
Histology	
ADC	79 (69.9)
SCC	34 (30.1)
Surgery	75 (66.4)
Surgery + chemotherapy	23 (20.4)
Surgery + radiation therapy	5 (4.4)
Surgery + chemo- and radiation therapy	10 (8.8)

ADC, adenocarcinoma; *SCC*, squamous cell carcinoma

Tumor masses were identified as areas of increased [^{18}F]FDG uptake in relation to normal lung parenchyma or other mediastinal structures. Tumor burden was calculated with three-dimensional volumes of interest (VOIs) drawn on the tumor-related activity volume by applying a percentage threshold of 42 %: maximum standardized uptake value (SUVmax) and SUVmean were defined as the highest pixel value and the mean uptake, respectively. Volumetric parameters included metabolic tumor volume (MTV), estimated from VOI SUV isoactivity contours automatically drawn using a fixed threshold (42 % SUVmax), and total lesion glycolysis (TLG), calculated as SUVmean× MTV.

Fractal Analysis

DICOM data retrieved from PET/CT scans were analyzed using a *ad hoc* computer-aided image analysis system (SWI Analyzer, Rozzano, Milan, Italy). The software (Fig. 1) automatically evaluates the following parameters: (a) mean intensity value (MIV), which defines the average gray values within the ROI. This is the sum of the gray values of all the pixels in the selection divided by the number of pixels, (b) standard deviation (SD), as a measure of the amount of variation or dispersion of the set of gray-levels within the ROI, (c) relative dispersion obtained by the ratio between the SD and the MIV of the gray-levels within the ROI, (d) 3D histogram fractal dimension (3D HIST FR DIM) as an estimate of the FD (*i.e.* grade of irregularity) of the histogram that identifies the gray-levels distribution within the ROI. The software generates the histogram using the quantity of pixels of specific gray-level as previously shown by Lopci, et al. [9], and (e) 3D fractal dimension (3D-FD), which defines the FD of the ROI 3D surface.

Two-dimensional (2D) and 3D-FDs were automatically estimated applying the box-counting algorithm, which uses the following equation:

$$D = \lim_{\varepsilon \to 0} \frac{logN(\varepsilon)}{\log\left(\frac{1}{\varepsilon}\right)}$$

where D is the box-counting FD of the object, ε is the side length of the 2D-box or 3D-box, and N(ε) is the smallest number of boxes of side ε required to cover the surface or the outline of the object completely. Fractal dimensions were estimated as D = d, where d is the gradient of the graph of log [N(ε)] against log 1/ε. The diagrams were then plotted and the linear correlation lines were identified using least squares regression method; their slopes were quantified using an "iterative resistant line method" [19] (Fig. 2).

Statistical Analysis

All variables were correlated with each other and to disease outcome expressed in terms of disease-free survival (DFS) over a median follow-up of 25.8 months. DFS was defined as the time from surgery until relapse, death, or the last visit where the patient was alive without recurrence. For survival analysis, we used the median values of metabolic and fractal parameters as the cut-off values. Relationships between FD and metabolic parameters were evaluated using Spearman's correlation analysis. For the univariate and multivariate analyses of survival, Cox's proportional hazard model was employed and the log-rank test with Kaplan–Meier analysis. The independent *t* test and Kruskal-Wallis test were used when appropriate.

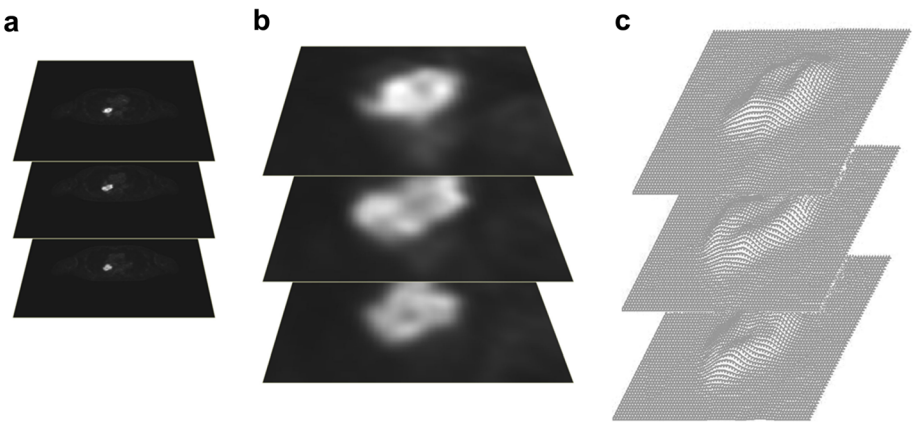

Fig. 1. **a** The computer-aided and fractal-based image analysis system automatically recognizes each ROI of the tumor lesion defined on the PET consecutive image level and **b** reconstructs the intra-tumoral heterogeneity as the sum of the gray-levels of all sequential image levels. **c** Subsequently, the software estimates three-dimensional fractal surface dimension, represented as a mesh, by applying the three-dimensional box-counting algorithm. The final obtained result is a fractional number, comprising between the Euclidean dimensions of two and three based on the spatial surface complexity.

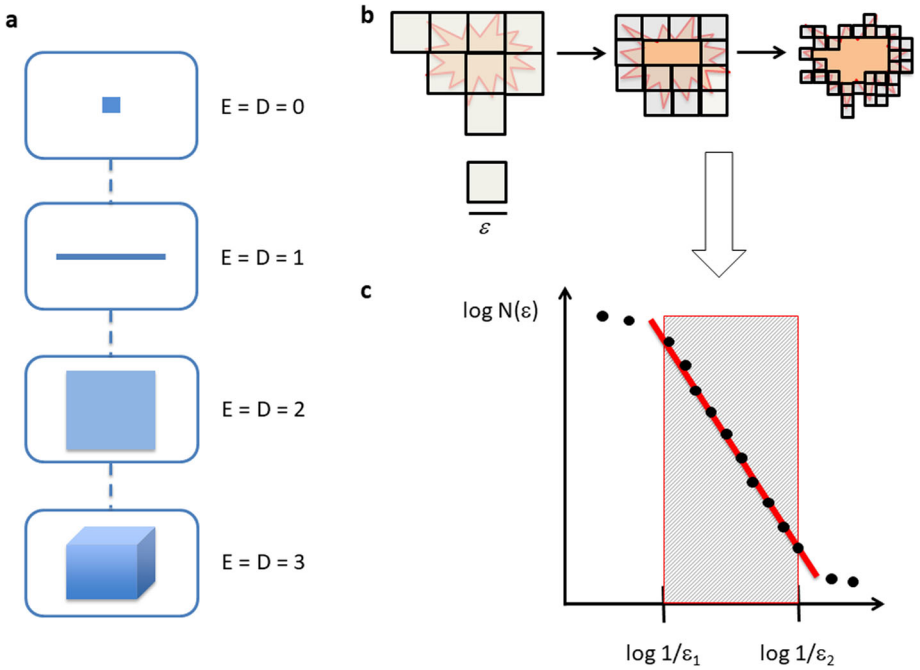

Fig. 2. **a** Dimension is a numerical attribute of an object that does not depend on its process of generation, and has been defined in two ways. The first is the topological or Euclidean dimension, which assigns an integer to every point or set of points in Euclidean space (E): 0 to a point (defined as that which has no part); 1 to a straight line (defined as a length without thickness), 2 to a plane surface (defined as having length and thickness, but no depth); and 3 to three-dimensional figures (a volume defined by length, thickness and depth). The second who attributed a real number to every natural object in E lying between the topological dimensions 0 and 3. **b** Fractal dimension has been estimated using the box-counting algorithm. Briefly, the method counts the number of boxes of length ε required to cover the surface or the outline of an irregularly-shaped object being measured, indicated as N(ε). **c** Prototypical curve is obtained that highlights the so-called "fractal windows" ranged by box size ε_1 and ε_2, and represents the appropriate region in which to estimate the dimension. Box sizes of more than ε_2 approach the size of the image until one box covers it completely, at which point N(ε) = 1 and the slope = 0. Box sizes smaller than ε_1 approach the resolution of the image: in this region, box counting simply gives the area of the image.

Differences between groups were compared by analysis of variance (ANOVA), when appropriate. All statistical analyses were carried out using the Statistical Package for Social Sciences, version 22.0, for Windows (SPSS, Chicago, IL), and p values < 0.05 were considered to be statistically significant.

Results

Histopathological examination diagnosed 79 lung adenocarcinomas (ADCs) and 34 squamous cell carcinomas (SCCs). Eighty-five patients were early stage (I and II), while 28 were locally advanced stage (III). Twenty-three patients underwent to adjuvant chemotherapy, five to radiation therapy after surgery, while 10 patients performed both chemotherapy and radiation therapy. The remnant patients (75/113) underwent directly to surgery and without further treatments. All evaluated tumor lesions were positive at [^{18}F]FDG PET/CT. The values of metabolic and fractal parameters derived from lung malignancies on DICOM images are depicted in Table 2.

Fractal Geometry-Based Analysis and [^{18}F]FDG PET/CT

Spearman's rank correlation analysis was performed with [^{18}F]FDG PET/CT metabolic parameters. Significantly positive correlations were found between 3D-FD and SUVmax (rho = 0.708, $p < 0.001$), SUVmean (rho = 0.671,

Table 2. Descriptive statistics of [^{18}F]FDG PET/CT parameters

Parameters	Median	Minimum	Maximum
SUVmax	11.1	2.2	39.4
SUVmean	6.2	1.5	13
MTV (ml)	8.3	1	365.4
TLG	56.6	1.6	3152.4
3D-FD	1.62	1.03	2.31
3D HIST FR DIM	0.2	0.03	2.38
MIV	155.1	10	209.8
SD	35	0	80.2
RD	0.3	0	0.96

SUV, standardized uptake value; *MTV*, metabolic tumor volume; *TLG*, total lesion glycolysis; *MIV*, mean intensity value; *SD*, standard deviation; *RD*, relative dispersion; *3D HIST FR DIM*, 3D histogram of the fractal dimension; *3D-FD* fractal dimension in 3D

$p < 0.001$), MTV (rho = 0.928, $p < 0.001$), and TLG (rho = 0.934, $p < 0.001$). Positive correlations between MIV, SD, and all metabolic parameters were also found (Table 3). Patients with high median 3D-FD (≥ 1.62) tumors showed higher values of SUVmax (16.9 *versus* 7.9, $p < 0.001$), SUVmean (8.5 *versus* 4.7, $p < 0.001$), MTV (53.6 *versus* 4.4, $p < 0.001$), and TLG (491.9 *versus* 21.6, $p < 0.001$). Furthermore, tumors with high median MIV (≥ 155.1) were associated with higher values of SUVmean, as well those with high median SD (≥ 35) with both SUVmax and SUVmean. No significant differences were found for RD and 3D HIST FR DIM parameters.

Univariate and Multivariate Analysis for DFS

On univariate analysis, median 3D-FD and median TLG resulted significantly associated with DFS ($p = 0.04$ and 0.03, respectively), while the median fractal geometry-based of other parameters and metabolic parameters including SUVmax, SUVmean, and MTV did not. These results were also confirmed by Kaplan–Meier analysis, where patients with low median 3D-FD (< 1.62) showed better DFS than those with higher median 3D-FD (DFS 50.1 *versus* 34.1 months, $p = 0.036$) (Fig. 3). Patients with low median TLG had a better DFS than those with greater TLG (DFS 58.3 *versus* 39.3 months, $p = 0.041$), while other parameters did not show a significant association with DFS. On multivariate analysis, only the median 3D-FD was found as independent prognostic factor for DFS ($p = 0.032$; HR 0.179, 95 % CI 0.038–0.834). Univariate and multivariate analyses for DFS are summarized in Table 4.

Two representative cases of patients with different 3D-FD values and outcomes are shown in Fig. 4.

Fractal Geometry-Based Analysis and Clinical Parameters

We found a significant difference ($p = 0.014$) between median 3D-FD values in ADCs and SSCs [1.44 (1.03–1.61) *versus* 1.94 (1.62–2.31)], respectively. While Kaplan-Meier curves show a trend for ADC patients to have a better DFS compared to SCC patients, the log-rank test revealed no statistical significance between the survival rates ($p = 0.116$) (Fig. 5). All other considered parameters (MIV, SD, RD, and 3D HIS FR DIM) showed no statistically significant difference between the two histotypes. Furthermore, according to disease stage, we found a statistically significant difference of 3D-FD, with higher 3D-FD values in the advanced stages ($p = 0.011$). On the other hand, no significant results were found for the remnant fractal parameters.

Discussion

Every biologic system, from macroscopic to sub-cellular objects, is characterized by irregularity in shape. While classical Euclidean geometry are not able to quantity such irregularity, fractal geometry has found a large application in numerous scientific sectors [19]. In general terms, four properties characterize a fractal object, as follows: (a) the irregularity of its shape; (b) the self-similarity of its structure; (c) its non-integer value or FD; and (d) scaling, which means that the measurement of its proprieties depends on the scale adopted. The most evident properties of any anatomical form are the irregularity of their shapes or the distribution patterns of a set of forms, which are substantially different from smooth Euclidean figures. Self-similarity can be geometrical or statistical. The first is defined when even the smaller piece of the object is an exact representation of the whole object, exemplified by the 'snowflake' of Niels Fabian Helge von Koch [19]. In contrast, statistical self-similarity also called "self-affinity" concerns biological, including anatomical entities. In fact, the components are rarely identical copies of the entire system [12, 19]. Taking advantages by this knowledge, we have developed a computer-aided fractal-based method capable to automatically estimate the tumor heterogeneity of [^{18}F]FDG PET/CT DICOM images taken from a series of NSCLC patients.

To the best of our knowledge, this is the first study aimed to evaluate spatial fractal analysis on [^{18}F]FDG PET/CT images to predict the prognosis of patients with NSCLC prior to surgery.

Table 3. Spearman's *rho* values obtained during the rank correlation analysis between semi-quantitative metabolic and fractal parameters

	SUVmax	SUVmean	MTV	TLG	3D FD	MIV	SD
SUVmax							
SUVmean	0.963*						
MTV	0.684*	0.621*					
TLG	0.819*	0.776*	0.973*				
3D FD	0.708*	0.671*	0.928*	0.934*			
MIV	0.342*	0.386*	0.236*	0.301*	0.354*		
SD	0.407*	0.399*	0.395*	0.430*	0.304*	− 0.140 (ns)	

SUV, standardized uptake value; *MTV*, metabolic tumor volume; *TLG*, total lesion glycolysis; *MIV*, mean intensity value; *SD*, standard deviation; *RD*, relative dispersion; *3D HIST FR DIM*, 3D histogram of the fractal dimension; *3D-FD* fractal dimension in 3D; *ns*, non-significant
*Significant correlation ($p < 0.05$)

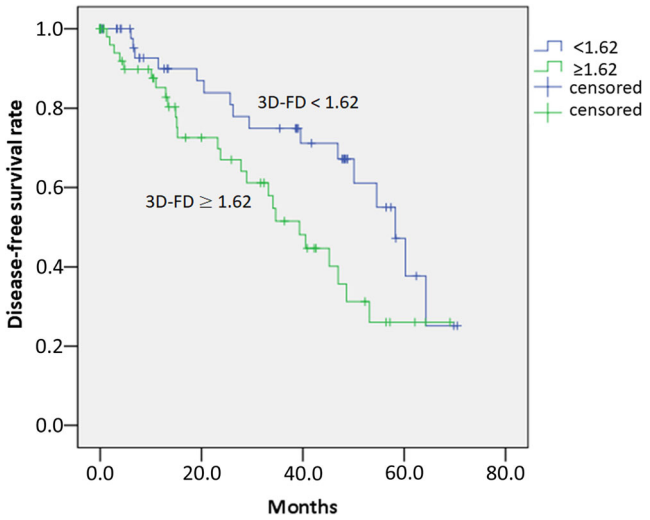

Fig. 3. In Kaplan–Meier analysis, low median 3D-FD was associated with favorable DFS.

Besides metabolic parameters extracted by [^{18}F]FDG PET/CT images, we adopted in addition a non-compartmental method to extrapolate fractal indices that represent tissue heterogeneity. FD has been estimated applying the box-counting algorithm [20]. It is known that whole-body PET/CT indices, including SUVmax, SUVmean, TLG, and MTV, might partially represent the total tumor heterogeneity. For example, SUVmax expresses the most biologically aggressive area, but it does not indicate its distribution within the tumor; moreover, malignant lesions with comparable metabolic values but different outcomes (Fig. 2) can be observed, highlighting the complexity and heterogeneity of tumoral lesions, which cannot be assessed when the "classical" PET/CT parameters are applied [21].

Table 4. Univariate and multivariate analyses of tumor parameters for DFS

Variable	Hazard ratio	95 % IC	*p* value
Univariate			
Age	1.003	0.962–1.046	0.88
T stage	1.210	0.843–1.736	0.30
N stage negative *vs* positive	0.942	0.508–1.746	0.85
Cancer stage	1.083	0.871–1.346	0.47
ADC *vs* SCC	1.603	0.842–3.054	0.15
Median SUVmax < 11.1 *vs* ≥ 11.1	1.868	0.978–3.569	0.06
Median SUVmean < 6.2 *vs* ≥ 6.2	0.626	0.328–1.195	0.16
Median MTV < 8.3 *vs* ≥ 8.3	0.636	0.342–1.185	0.15
Median TLG < 56.6 *vs* ≥ 56.6	0.439	0.214–0.903	*0.03**
Median 3D FD < 1.62 *vs* ≥ 1.62	0.513	0.272–0.967	*0.04**
Median MIV < 155.1 *vs* ≥ 155.1	0.718	0.384–1.342	0.29
Median SD < 35 *vs* ≥ 35	0.807	0.436–1.493	0.49
Median RD < 0.3 *vs* ≥ 0.3	1.211	0.648–2.261	0.55
Median 3D HIS FR DIM < 0.2 *vs* ≥ 0.2	0.952	0.510–1.777	0.88
Multivariate			
3D FD < 1.62 *vs* ≥ 1.62	0.179	0.038–0.834	*0.03**

ADC, adenocarcinoma; *SCC*, squamous cell carcinoma; *SUV*, standardized uptake value; *MTV*, metabolic tumor volume; *TLG*, total lesion glycolysis; *MIV*, mean intensity value; *SD*, standard deviation; *RD*, relative dispersion; *3D HIST FR DIM*, 3D histogram of the fractal dimension; *3D-FD*, fractal dimension in 3D. *$p < 0.05$

Tumor heterogeneity, however, can be a novel independent biomarker for cancer patients. It represents an estimate of the [^{18}F]FDG uptake and distribution pattern. Several researchers have reported the tumor structural heterogeneity as an important factor for the prediction of cancer progression. It is hypothesized that various factors, including vascularization, hypoxia, cancer microenvironment, or necrosis determine the tumor heterogeneity, progression, development of distant metastases or resistance to therapies [22–29].

In our study, 3D-FD was found statistically correlated with [^{18}F]FDG PET/CT parameters, *i.e.* SUVmax ($r = 0.708$), SUVmean ($r = 0.671$), MTV ($r = 0.928$) and TLG ($r = 0.934$). Additionally, MIV and SD were correlated with the same metabolic parameters (Table 3). These high correlations values between fractal indices and metabolic parameters agree with previous studies in NSCLC and multiple myeloma patients, although in these studies FD was calculated for the time-activity data and not for spatial data [16, 30]. Dimitrakopoulou-Strauss, et al. [16] performed a double-tracer PET/CT study with [^{18}F]FDG and fluorine-18-fluoromisonidazole in patients with advanced NSCLC scheduled for radiation therapy and found a high correlation between FD and various SUV parameters, for both radiotracers. The same group demonstrated a statistically significant correlation with SUVaverage both in [^{18}F]FDG as well as in sodium [^{18}F]fluoride PET/CT examinations. Since both FD of the time-activity data and SUVs were enhanced in malignancies, they suggested that the application of non-compartment derived parameters could aid in evaluating complicated oncological differential diagnoses [30]. Additionally, by applying compartmental and non-compartmental analysis the shape of the tracer time activity curve (*i.e.* a set of continuous dynamical points) can be estimated by its fractal dimension and, therefore, additional valuable information concerning the influx and efflux of [^{18}F]FDG, as well as phosphorylation and dephosphorylation rate can be obtained [31].

In the prediction of prognosis, we found that at the multivariate analysis 3D-FD is an independent predictive factor for DFS in resectable NSCLC patients. This result is consistent with other studies, which demonstrated that "structural complexity" is associated with a poor prognosis in lung, sarcoma and esophageal cancer [32–34]. High 3D-FD on [^{18}F]FDG PET/CT images might reflect an aggressive biology of the tumor, since malignant tumors include a mixture of functionally distinct cell populations with completely different behaviors.

Moreover, our study shows that 3D-FD may be used to differentiate between ADCs and SCCs, as ADCs have a lower 3D-FD. Lee et al. [35] has shown that FD was helpful in differentiating those two most common lung cancer histotypes on digitally imaged samples of resected NSCLC tumors but not on [^{18}F]FDG PET/CT images.

Based on our results, we can hypothesize that 3D-FD depends on the histopathological features. Tumor

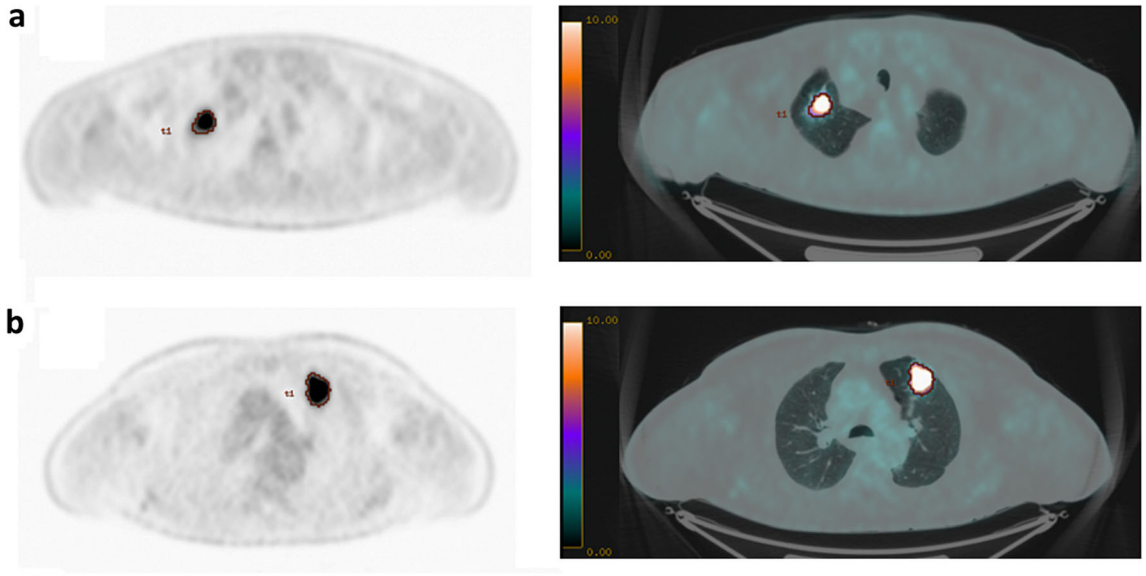

Fig. 4. Two patients with lung cancer, both pT2 N0 M0. SUVmax were almost the same (about 17) for both patients, but 3D-FD was 1.60 (**a**) and 1.88 (**b**), respectively. Patient (**a**) had a disease-free survival of 48 months. Patient (**b**) a disease-free survival of 12 months.

heterogeneity, expressed by 3D-FD of NSCLC PET images, can be a potential biomarker capable to categorize NSCLCs in ADCs and SCCs subtypes. This aspect may be of primary importance in the patient's management, as 3D-FD is obtained using a computer-aided image analysis system totally independent by the operator. 3D-FD might also be useful in the development of new and more sophisticate algorithms for the digital assessment of cancer morphology. We also found higher 3D-FD values in advanced disease stages, which may be correlated with more aggressive behavior, worse response to treatment, and definitively, worse prognosis as demonstrated in other solid and non-solid tumors [32, 36–39]. This feature might find its utility in patients with stage IV disease where lung surgery cannot be performed. Previously, fractal geometry was applied to differentiate malignant from benign pulmonary nodules [15]. Apparently, in contrast to our results, Miwa et al. found that FD was lower for malignant lesions compared to benign pulmonary nodules, although they did not take into account histological types or inflammatory conditions.

This study has, however, two limitations. First, it is a retrospective analysis based on a single center dataset. Secondly, we evaluated the heterogeneity of the primary tumor, but not in the involved lymph nodes.

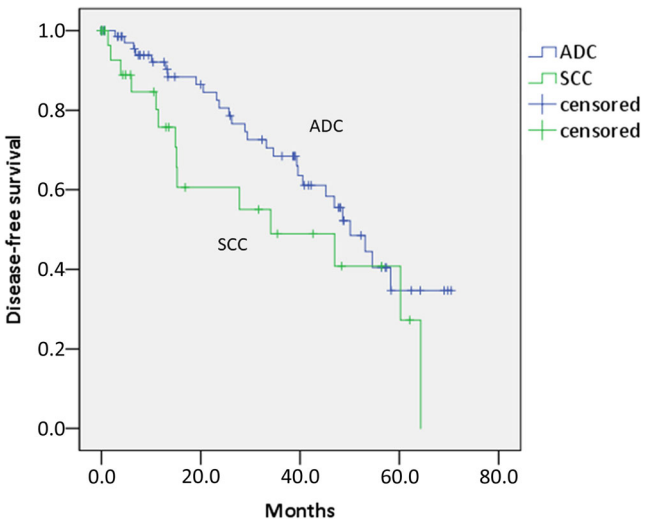

Fig. 5. Kaplan–Meier curves show a longer DFS for patients with ADCs, although log-rank test was not significant.

Conclusions

In this study, the intra-tumoral heterogeneity of [^{18}F]FDG PET/CT images as represented by 3D-FD can be a useful prognostic biomarker for DFS in patients with NSCLC, independently by clinical markers. By combining metabolic parameters and fractal geometry from [^{18}F]FDG PET/CT images, we might provide clinically relevant information and important insights for patient's management.

Acknowledgments. The Italian Association for Research on Cancer (AIRC—Associazione Italiana per la Ricerca sul Cancro) is acknowledged for the support on research with the grant nr. 18923. The "Michele Rodriguez" Foundation is also acknowledged for the scientific support.

Compliance with Ethical Standards. The study was approved by the institutional review board and conducted according to the guidelines of the institutional review board and to good clinical practice according to the ethical principles that have their origin in the Declaration of Helsinki.

Conflict of Interest

The authors declare that they have no conflict of interest.

References

1. American Cancer Society (2018) Cancer facts and figures 2018. American Cancer Society, Atlanta Available via https://www.cancer.org/research/cancer-facts-statistics/all-cancer-facts-figures/cancer-facts-figures-2018.html
2. Siegel RL, Miller KD, Jemal A (2018) Cancer statistics, 2018. CA Cancer J Clin 68:7–30
3. Gould MK, Maclean CC, Kuschner WG, Rydzak CE, Owens DK (2001) Accuracy of positron emission tomography for diagnosis of pulmonary nodules and mass lesions: a meta-analysis. JAMA 285:914–924
4. Lardinois D, Weder W, Hany TF, Kamel EM, Korom S, Seifert B, von Schulthess GK, Steinert HC (2003) Staging of non-small-cell lung cancer with integrated positron-emission tomography and computed tomography. N Engl J Med 348:2500–2507
5. Feng M, Yang X, Ma Q, He Y (2017) Retrospective analysis for the false positive diagnosis of PET-CT scan in lung cancer patients. Medicine (Baltimore) 96:e7415
6. Sugama C, Vicky G, Musib S et al (2013) Quantifying tumour heterogeneity in ^{18}F-FDG PET/CT imaging by texture analysis. Eur J Nucl Med Mol Imaging 40:133–140
7. Cook GJ, Yip C, Siddique M et al (2013) Are pretreatment ^{18}F-FDG PET tumor textural features in non-small cell lung cancer associated with response and survival after chemoradiotherapy? J Nucl Med 54:19–26
8. Tin HW, Leu SW, Sasaki H, Chang SH (2014) A novel fractal block coding method by using new shape-based descriptor. Appl Math Inform Sci 8:849–855
9. Lopci E, Grizzi F, Russo C, Toschi L, Grassi I, Cicoria G, Lodi F, Mattioli S, Fanti S (2017) Early and delayed evaluation of solid tumours with ^{64}Cu-ATSM PET/CT: a pilot study on semiquantitative and computer-aided fractal geometry analysis. Nucl Med Commun 38:340–346
10. Sedivy R (1996) Fractal tumours: their real and virtual images. Wien Klin Wochenschr 108:547–551
11. Mandelbrot B (1967) How long is the coast of Britain? Statistical self-similarity and fractal dimension. Science 156:636–638
12. Grizzi F, Castello A, Qehajaj D, Russo C, Lopci E (2018) The complexity and fractal geometry of nuclear medicine images. Mol Imaging Biol. https://doi.org/10.1007/s11307-018-1236-5
13. Kikuchi A, Kozuma S, Yasugi T, Taketani Y (2004) Fractal analysis of surface growth patterns in endometrioid endometrial adenocarcinoma. Gynecol Obstet Investig 58:61–67
14. Vasiljevic J, Reljin B, Sopta J, Mijucic V, Tulic G, Reljin I (2012) Application of multifractal analysis on microscopic images in the classification of metastatic bone disease. Biomed Microdevices 14:541–548
15. Miwa K, Inubushi M, Wagatsuma K, Nagao M, Murata T, Koyama M, Koizumi M, Sasaki M (2014) FDG uptake heterogeneity evaluated by fractal analysis improves the differential diagnosis of pulmonary nodules. Eur J Radiol 83:715–719
16. Dimitrakopoulou-Strauss A, Hoffmann M, Bergner R, Uppenkamp M, Eisenhut M, Pan L, Haberkorn U, Strauss LG (2007) Prediction of short-term survival in patients with advanced non small cell lung cancer following chemotherapy based on 2-deoxy-2-[F-18]fluoro-D-glucose-positron emission tomography: a feasibility study. Mol Imaging Biol 9:308–317
17. Sachpekidis C, Thieke C, Askoxylakis V et al (2015) Combined use of ^{18}F-FDG and ^{18}F-FMISO in unresectable non-small cell lung cancer patients planned for radiotherapy: a dynamic PET/CT study. Am J Nucl Med Mol Imaging 5:127–142
18. Boellaard R, Delgado-Bolton R, Oyen WJ, Giammarile F et al (2015) FDG PET/CT: EANM procedure guidelines for tumour imaging: version 2.0. Eur J Nucl Med Mol Imaging 42:328–354
19. Di Ieva A, Grizzi F, Jelinek H et al (2013) Fractals in the neurosciences, part I: general principles and basic neurosciences. Neuroscientist 20:403–417
20. Dimitrakopoulou-Strauss A, Strauss LG, Mikolajczyk K et al (2003) On the fractal nature of dynamic positron emission tomography (PET) studies. World J Nucl Med 2:306–313
21. Watabe T, Tatsumi M, Watabe H, Isohashi K, Kato H, Yanagawa M, Shimosegawa E, Hatazawa J (2012) Intratumoral heterogeneity of F-18 FDG uptake differentiates between gastrointestinal stromal tumors and abdominal malignant lymphomas on PET/CT. Ann Nucl Med 26:222–227
22. Hayano K, Lee SH, Yoshida H, Zhu AX, Sahani DV (2014) Fractal analysis of CT perfusion images for evaluation of antiangiogenic treatment and survival in hepatocellular carcinoma. Acad Radiol 21:654–660
23. Carmeliet P, Jain RK (2011) Molecular mechanisms and clinical applications of angiogenesis. Nature 473:298–307
24. Matsumoto S, Batra S, Saito K, Yasui H, Choudhuri R, Gadisetti C, Subramanian S, Devasahayam N, Munasinghe JP, Mitchell JB, Krishna MC (2011) Antiangiogenic agent sunitinib transiently increases tumor oxygenation and suppresses cycling hypoxia. Cancer Res 71:6350–6359
25. Calderwood SK (2013) Tumor heterogeneity, clonal evolution, and therapy resistance: an opportunity for multitargeting therapy. Discov Med 15:188–194
26. Marusyk A, Polyak K (2010) Tumor heterogeneity: causes and consequences. Biochim Biophys Acta 1805:105–117
27. Vogelstein B, Papadopoulos N, Velculescu VE, Zhou S, Diaz LA, Kinzler KW (2013) Cancer genome landscapes. Science 339:1546–1558
28. Gupta RG, Somer RA (2017) Intratumor heterogeneity: novel approaches for resolving genomic architecture and clonal evolution. Mol Cancer Res 15:1127–1137
29. Pribluda A, de la Cruz CC, Jackson EL (2015) Intratumoral heterogeneity: from diversity comes resistance. Clin Cancer Res 21:2916–2923
30. Sachpekidis C, Goldschmidt H, Hose D, Pan L, Cheng C, Kopka K, Haberkorn U, Dimitrakopoulou-Strauss A (2014) PET/CT studies of multiple myeloma using ^{18}F-FDG and ^{18}F-NaF: comparison of distribution patterns and tracers' pharmacokinetics. Eur J Nucl Med Mol Imaging 41:1343–1353
31. Sachpekidis C, Anwar H, Winkler JK et al (2018) Longitudinal studies of the ^{18}F-FDG kinetics after ipilimumab treatment in metastatic melanoma patients based on dynamic FDG PET/CT. Cancer Immunol Immunother. https://doi.org/10.1007/s00262-018-2183-3
32. Tixier F, Vriens D, Cheze-Le Rest C et al (2016) Comparison of tumor uptake heterogeneity characterization between static and parametric ^{18}F-FDG PET images in non-small cell lung cancer. J Nucl Med 57:1033–1039
33. Okazumi S, Dimitrakopoulou-Strauss A, Schwarzbach MH, Strauss LG (2009) Quantitative, dynamic ^{18}F-FDG-PET for the evaluation of soft tissue sarcomas: relation to differential diagnosis, tumor grading and prediction of prognosis. Hell J Nucl Med 12:223–228
34. Tochigi T, Shuto K, Kono T, Ohira G, Tohma T, Gunji H, Hayano K, Narushima K, Fujishiro T, Hanaoka T, Akutsu Y, Okazumi S, Matsubara H (2017) Heterogeneity of glucose metabolism in esophageal cancer measured by fractal analysis of fluorodeoxyglucose positron emission tomography image: correlation between metabolic heterogeneity and survival. Dig Surg 34:186–191
35. Lee LH, Tambasco M, Otsuka S, Wright A, Klimowicz A, Petrillo S, Morris D, Magliocco A, Bebb DG (2014) Digital differentiation of non-small cell carcinomas of the lung by the fractal dimension of their epithelial architecture. Micron 67:125–131
36. Eary JF, O'Sullivan F, O'Sullivan J, Conrad EU (2008) Spatial heterogeneity in sarcoma 18F FDG uptake as a predictor of patient outcome. J Nucl Med 49:1973–1979
37. Tixier F, Le Rest CC, Hatt M et al (2011) Intratumor heterogeneity characterized by textural features on baseline ^{18}F-FDG PET images predicts response to concomitant radiochemotherapy in esophageal cancer. J Nucl Med 52:369–378
38. Lee M, Lee H, Cheon GJ, Kim HS, Chung HH, Kim JW, Park NH, Song YS (2017) Prognostic value of preoperative intratumoral FDG uptake heterogeneity in patients with epithelial ovarian cancer. Eur Radiol 27:16–23
39. Ceriani L, Milan L, Martelli M, Ferreri AJM, Cascione L, Zinzani PL, di Rocco A, Conconi A, Stathis A, Cavalli F, Bellei M, Cozens K, Porro E, Giovanella L, Johnson PW, Zucca E (2018) Metabolic heterogeneity on baseline ^{18}FDG-PET/CT scan is a predictor of outcome in primary mediastinal B-cell lymphoma. Blood 132:179–186. https://doi.org/10.1182/blood-2018-01-826958